Critical phenomenon of the single crystal helimagnet MnSi

Lei Zhang,[1,*] Dirk Menzel,[2] Chiming Jin,[1] Haifeng Du,[1,†] Min Ge,[3]
Changjin Zhang,[1] Li Pi,[1,3] Mingliang Tian,[1] and Yuheng Zhang[1,3]

[1]*High Magnetic Field Laboratory, Chinese Academy of Sciences, Hefei 230031, China*

[2]*Institut für Physik der Kondensierten Materie,*
Technische Universität Braunschweig, D-38106 Braunschweig, Germany

[3]*Hefei National Laboratory for Physical Sciences at the Microscale,*
University of Science and Technology of China, Hefei 230026, China

(Dated: December 8, 2014)

Abstract

The critical behavior of the single crystal helimagnet MnSi is investigated by means of bulk dc-magnetization at the boundary between the conical state and paramagnetic phase. We obtain the critical exponents ($\beta = 0.242 \pm 0.006$, $\gamma = 0.915 \pm 0.003$, and $\delta = 4.734 \pm 0.006$), where the self-consistency and reliability are verified by the Widom scaling law and the scaling equation. The critical exponents of MnSi belong to the universality class of tricritical mean-field theory, which unambiguously indicates a tricritical phenomenon at the boundary between the first-order phase transition and the second-order one induced by the external magnetic field. The tricritical point (TCP) is determined as $H_{TCP} \approx 3200$ Oe at the critical temperature, consistent with the previous report [Phys. Rev. Lett. **110,** 177207 (2013)]. The critical behavior suggests a long-range magnetic coupling with the exchange distance decaying as $J(r) \approx r^{-4.3}$ in MnSi.

PACS numbers: 75.40.-s, 75.40.Cx, 75.40.Gb

Keywords: helimagnetism; critical phenomenon; tricritical point

*Corresponding author. Email: zhanglei@hmfl.ac.cn

†Corresponding author. Email: duhf@hmfl.ac.cn

I. INTRODUCTION

For decades, the B20 transition metal compound MnSi has always been fascinating due to its weak itinerant ferromagnetism [1], non-Fermi-liquid behavior [2, 3], and magnetic quantum phase transition [4]. Recently, there is a renewed interest in MnSi because of the discovery of the skyrmion phase [5, 6, 7, 8, 9, 10, 11], which has great potential for new spin-based applications on account of the topological property [5, 6], nanometric size [12, 13], and current-driven motion [14, 15, 16, 17]. The crystal structure of MnSi is a non-centrosymmetric cubic cell with space group $P2_13$, which results in a weak Dzyaloshinskii-Moriya (DM) spin-orbit coupling due to the lack of inversion symmetry. The DM spin-orbit coupling competes with the much stronger ferromagnetic exchange, which finally causes a long modulation period of a helimagnetic ground state [5, 6, 18]. When an external magnetic field is applied above a threshold value, the helimagnetic state transforms into a conical phase [19]. The chiral skyrmion phase emerges just below T_C in a narrow magnetic field range due to a unique stabilization provided by the DM interactions [5]. The ordering processes in cubic helimagnets are characterized by the formation of specific precursor states [18, 20]. It is demonstrated that a disordered Skyrmion phase appears in a very narrow temperature range of ~ 1 K above the helical phase in MnSi [21, 22, 23].

Recently, the critical phenomena of some helimagnets with a skyrmion phase have been analyzed intensively to investigate the detailed ferromagnetic exchange. For example, it has been demonstrated that the near-neighbor isotropic exchange of short-range type is dominant in $Fe_{0.8}Co_{0.2}Si$ [24]. In addition, another multiferroic insulating helimagnet Cu_2OSeO_3, which also exhibits a skyrmion state, is consistent with the classical three-dimensional (3D) Heisenberg model with short-range interaction [25]. However, for MnSi, the magnetic exchange is expected to be different from that in $Fe_{1-x}Co_xSi$ or Cu_2OSeO_3 because a long-range coupling as described by the mean-field theory has been predicted by the theory of Brazovskii [26]. According to the Brazovskii scenario, a first-order phase transition from paramagnetic to helimagnetic ordering was induced by the critical fluctuation under zero-field [26], which is supported experimentally by the neutron scattering studies [27], the renormalization group theory [18] and Monte Carlo simulations [28]. The weak first-order phase transition can be suppressed into a second-order one by the external magnetic field, prospectively yielding tricritical behavior [29, 30]. However, the tricritical phenomenon of this system has not been

studied in detail. In this work, the critical behavior of the single crystal MnSi is investigated around T_C by means of bulk dc-magnetization. We find that the critical exponents of MnSi satisfy the universality class of the tricritical mean-field theory, which unambiguously indicates a tricritical phenomenon at the boundary of the first-order transition and the second-order one. The tricritical point is determined to be $H_{TCP} \approx 3200$ Oe at T_C, which agrees with the results of specific heat experiments [30]. Moreover, the critical behavior indicates a long-range magnetic coupling with the magnetic exchange distance decaying as $J(r) \approx r^{-4.3}$.

II. EXPERIMENT

A single crystal sample of MnSi was prepared by the Czochralski method [31]. The structure and phase purity were checked with a Rigaku-TTR3 X-ray diffractometer. The chemical compositions were carefully determined by energy dispersive x-ray spectrometry (EDXS), which shows the proportion of Mn : Si $\approx 49 : 51$. The magnetization was measured using a Quantum Design vibrating sample magnetometer (SQUID-VSM). The no-overshoot mode was applied to ensure a precise magnetic field. In addition, the field was relaxed for 2 minutes before the data collection. For the measurement the sample was processed into slender ellipsoid shape, and the magnetic field was applied along the longest axis to minimize the demagnetizating field. To make sure each curve was initially magnetized, the isothermal magnetization was performed after the sample was heated well above T_C for 10 minutes and then cooled under zero field to the target temperatures. The magnetic background was carefully subtracted. The applied magnetic field H_a has been corrected into the internal field as $H = H_a - NM$ (where M is the measured magnetization and N is the demagnetization factor) [32]. The corrected H was used for the analysis of critical behavior.

III. RESULTS AND DISCUSSION

Figure 1 (a) shows the temperature dependence of magnetization $M(T)$ for MnSi under zero-field-cooling (ZFC) and field-cooling (FC) with $H = 100$ Oe (left coordinate). A paramagnetic-helimagnetic (PM-HM) transition occurs at $T_C = 30.5$ K determined by dM/dT (right coordinate), which agrees with the expected mean-field transition tempera-

ture $T_{MF} \approx 30.5$ K [27, 33]. A narrow dip appears at ~ 29.7 K just below T_C (see the inset of Fig. 1 (a)), which is a clue to the first-order phase transition. Figure 1 (b) gives the isothermal magnetization $M(H)$ at 4 K, which exhibits a magnetic ordering behavior with the saturation field $H_S \sim 6000$ Oe. The inset of Fig. 1 (b) plots the magnification of $M(H)$ in the lower field region, which indicates almost no coercive force for MnSi.

As is well known, the critical behavior for a second-order phase transition can be investigated in detail through a series of critical exponents. In the vicinity of a second-order phase transition, the divergence of correlation length $\xi = \xi_0|(T - T_C)/T_C|^{-\nu}$ leads to universal scaling laws for the spontaneous magnetization M_S and initial susceptibility χ_0. The mathematical definitions of the exponents from magnetization are described as [34, 35]:

$$M_S(T) = M_0(-\varepsilon)^{\beta}, \varepsilon < 0, T < T_C \tag{1}$$

$$\chi_0^{-1}(T) = (h_0/M_0)\varepsilon^{\gamma}, \varepsilon > 0, T > T_C \tag{2}$$

$$M = DH^{1/\delta}, \varepsilon = 0, T = T_C \tag{3}$$

where $\varepsilon = (T - T_C)/T_C$ is the reduced temperature; M_0/h_0 and D are critical amplitudes. The parameters β (associated with M_S), γ (associated with χ_0), and δ (associated with T_C) are the critical exponents. Generally, the critical exponents should follow the Arrott-Noakes equation of state [36]:

$$(H/M)^{1/\gamma} = (T - T_C)/T_C + (M/M_1)^{1/\beta} \tag{4}$$

Therefore, the critical exponents β and γ can be obtained by fitting the $M_S(T)$ and $\chi_0^{-1}(T)$ curves using the modified Arrott plot of $M^{1/\beta}$ vs $(H/M)^{1/\gamma}$. Meanwhile, the third exponent δ can be generated directly by Eq. (3).

For the analysis of the critical behavior, we measure the initial isothermal $M(H)$ curves around T_C, which are shown in Fig. 2 (a). Previous theoretical investigation suggested that magnetic coupling in MnSi should be described using the mean-field theory [26]. In the mean-field theory where $\beta = 0.5$ and $\gamma = 1.0$ [37], we generate the Arrott plot of M^2 vs H/M, as shown in Fig. 2 (b). Generally, M^2 vs H/M should be a series of parallel straight lines in the higher field range. The lower field data, which mainly represent the arrangement

of magnetic domains, should be excluded in the fitting process [38]. The line of M^2 vs H/M at T_C should pass through the origin [39]. According to the criterion proposed by Banerjee, the order of the magnetic transition can be determined from the slope of the straight line: a positive slope corresponds to the second-order transition while the negative to the first-order one [40]. Apparently, the positive slopes of the present M^2 vs H/M curves imply that the magnetic transition of MnSi in the higher field region is a second-order one. However, all the curves in the Arrott plot are nonlinear and show downward curvature even in the high field region, in agreement with previous report [41]. This suggests that the mean-field theory with β= 0.5 and γ= 1.0 is not appropriate for MnSi according to the Arrott-Noakes equation of state [36]. Hence, a modified Arrott plot should be employed to obtain the critical exponents.

Three kinds of possible exponents belonging to the 3D-Heisenberg model (β= 0.365, γ=1.336), 3D-Ising model (β= 0.325, γ=1.24), and tricritical mean-field model (β= 0.25, γ=1.0) are used to make a modified Arrott plot, as shown in Fig. 3 (a), (b), and (c). All three models exhibit quasi-straight lines in the high field region [42, 43, 44]. To determine an appropriate model, the modified Arrott plots should be a series of parallel lines in the high field region with the same slope (where the slope is defined as $S(T) = dM^{1/\beta}/d(H/M)^{1/\gamma}$). The normalized slope (NS) is defined as $NS = S(T)/S(T_C)$, which enables one to identify the most suitable model by comparing NS with the ideal value of '1' [42]. Plots of NS vs T for the three different models are shown in Fig. 3 (d), which indicates that the tricritical mean-field model is the best one to describe the critical behavior of MnSi.

The linear extrapolation from the high field region to the intercepts with the axes $M^{1/\beta}$ and $(H/M)^{1/\gamma}$ yields reliable values of spontaneous magnetization $M_S(T, 0)$ and inverse initial susceptibility $\chi_0^{-1}(T, 0)$, which are plotted as a function of temperature in Fig. 4 (a). By fitting to Eq. (1) and Eq. (2), one obtains $\beta = 0.242 \pm 0.006$ with $T_C = 30.38 \pm 0.04$ and $\gamma = 0.915 \pm 0.003$ with $T_C = 30.69 \pm 0.07$. The critical temperature T_C from the modified Arrott plot is very close to that obtained from the $M(T)$ curve. Figure 4 (b) shows the isothermal magnetization $M(H)$ at $T_C = 30.5$ K, where the inset plots are on a $\lg - \lg$ scale. We determine that $\delta = 4.734 \pm 0.006$ in the high field region ($H > H_S$). It can be seen that the $M(H)$ at T_C exhibits a straight line on a $\lg - \lg$ scale for $H > H_S$. According to

statistical theory, these critical exponents should fulfill the Widom scaling relation [45]:

$$\delta = 1 + \frac{\gamma}{\beta} \tag{5}$$

As a result, $\delta = 4.781 \pm 0.007$ is calculated following the Widom scaling relation based on the obtained β and γ, which agrees well with the results from the experimental critical isothermal analysis. The self-consistency of these critical exponents demonstrates that they are reliable and unambiguous. In order to further testify the convergence of the critical exponents, the effective exponents β_{eff} and γ_{eff} for MnSi are obtained as [46]:

$$\beta_{eff}(\varepsilon) = \frac{d[lnM_S(\varepsilon)]}{d(ln\varepsilon)}, \gamma_{eff}(\varepsilon) = \frac{d[ln\chi_0^{-1}(\varepsilon)]}{d(ln\varepsilon)} \tag{6}$$

The effective exponents β_{eff} and γ_{eff} as a function of reduced temperature ε for MnSi are plotted in Fig. 5. It can be seen that β_{eff} and γ_{eff} are convergent when the temperature approaches T_C.

The obtained critical exponents of MnSi, as well as those from different theoretical models and related materials, are listed in Table I for comparison. It can be seen that the exponents of MnSi are very close to those predicted by the tricritical mean-field theory, which unambiguously indicates a tricritical phenomenon. The tricritical phenomenon usually occurs at the boundary between a first-order phase transition and a second-order one, where the three lines of critical transitions meet at a single point: the so called tricritical point (TCP) [47, 48, 49]. In the manganese oxides, the tricritical phenomenon usually occurs when the first-order phase transition disappears and the second-order transition is induced by proper doping effects [47, 48, 49]. In the present case of MnSi, a similar phase transition from first-order to second-order also occurs. It should be noted that an isotropic critical fluctuation induced first-order phase transition happens to MnSi under zero field, which can be easily suppressed by an external magnetic field [18, 19, 27, 28]. Thus, in this case, the tricritical phenomenon is expected at the boundary of these two phases. The critical point appears when the first-order phase transition is suppressed into a second-order one by an external field. The existence of a field-induced tricritical phenomenon was also pointed out by A. Bauer *et al.* in terms of the high-precision measurement of the specific heat [30]. In fact, high pressures can also induced a tricritical behavior in MnSi with $P_{tr} \approx 3.5$ GPa and $T_{tr} \approx 25$ K, where the pressure modulates the orders of the phase transitions [50, 51, 52]. The critical exponents obtained here in the single crystal sample are slightly different from

those in the polycrystalline one, where the exponent δ was calculated using the Widom scaling relation rather than obtained from the experiment [53]. As can be seen in Table I, the exponents obtained in the polycrystalline sample cannot be categorized into any universality classes, which may be attributed to the magnetic scattering from lots of crystal boundaries and defects. As we know, when the temperature approaches to the critical point, the correlation length ξ exceeds the grain size, where the critical exponents are affected by the crystal boundaries and defects [54]. Thus, the intrinsic magnetic coupling is masked in an inhomogeneous polycrystalline sample, especially for the long-range interaction [54].

The agreement of MnSi with the tricritical mean-field model indicates a long-range magnetic coupling which is revealed by the exponent γ [55]. As we know, for a homogeneous magnet, the universality class of the magnetic phase transition depends on the exchange distance $J(r)$. M. E. Fisher *et al*. theoretically treated this kind of magnetic ordering as an attractive interaction of spins, where a renormalization group theory analysis suggests the interaction decays with distance r as [55, 56]:

$$J(r) \approx r^{-(d+\sigma)} \tag{7}$$

were d is the spatial dimensionality and σ is a positive constant. Moreover, there is [32, 55, 57]:

$$\gamma = 1 + \frac{4}{d}\frac{n+2}{n+8}\Delta\sigma + \frac{8(n+2)(n-4)}{d^2(n+8)^2}\left[1 + \frac{2G(\frac{d}{2})(7n+20)}{(n-4)(n+8)}\right]\Delta\sigma^2 \tag{8}$$

where $\Delta\sigma = (\sigma - \frac{d}{2})$ and $G(\frac{d}{2}) = 3 - \frac{1}{4}(\frac{d}{2})^2$, n is the spin dimensionality. For a three dimensional material ($d = 3$), we have $J(r) \approx r^{-(3+\sigma)}$. When $\sigma \geq 2$, the Heisenberg model ($\beta = 0.365$, $\gamma = 1.386$ and $\delta = 4.8$) is valid for the three dimension isotropic magnet, where $J(r)$ decreases faster than r^{-5}. When $\sigma \leq 3/2$, conditions for the the mean-field model ($\beta = 0.5$, $\gamma = 1.0$ and $\delta = 3.0$) are satisfied, expecting that $J(r)$ decreases slower than $r^{-4.5}$. From Eq. 8 we see that $\sigma = 1.329 \pm 0.008$ for MnSi, thus confirming the long-range magnetic coupling for $\sigma < 3/2$. Subsequently, we find that the exchange distance decays as $J(r) \approx r^{-4.3}$, which indicates slow decay of the magnetic coupling. The decay distant of MnSi suggests that the spatial magnetic interaction is relatively extensive. Moreover, we get the correlation length critical exponent $\nu = 0.688 \pm 0.009$ (where $\nu = \gamma/\sigma$), which is close to 0.62 ± 1 obtained by small-angle polarized neutron scattering (SAPNS) [58].

Finally, these critical exponents should follow the scaling equation. According to the prediction of scaling equation, in the asymptotic critical region, the magnetic equation can

be written as [34]:

$$M(H,\varepsilon) = \varepsilon^{\beta} f_{\pm}(H/\varepsilon^{\beta+\gamma}) \tag{9}$$

where $f_{\pm}$ are regular functions denoted as f_{+} for $T > T_C$ and f_{-} for $T < T_C$. Defining the renormalized magnetization as $m \equiv \varepsilon^{-\beta} M(H,\varepsilon)$, and the renormalized field as $h \equiv H\varepsilon^{-(\beta+\gamma)}$), the scaling equation indicates that m vs h forms two universal curves for $T > T_C$ and $T < T_C$, respectively [49, 54]. Based on the scaling equation [$m = f_{\pm}(h)$], the isothermal magnetization around the critical temperatures for MnSi is plotted in Fig. 6 (a), where all experimental data in the higher field region collapse onto two universal curves. In addition, the experimental data in low field region above T_C collapse well. However, the lower-field experimental data below T_C cannot collapse onto one curve, as shown in the inset of Fig. 6 (a). The m^2 vs h/m curves [Fig. 6 (b)] apparently exhibit a vertical line in the lower field region. As we know, MnSi exhibits a first-order phase transition under a low external magnetic field, which is suppressed into a second-order one with a strong external field. The TCP of magnetic field (H_{TCP}) lies at the boundary between the first-order and the second-order transition. Above H_{TCP} in the second-order transition region, the $M-T-H$ curves should collapse onto a universal curve. However, below H_{TCP} in the first-order transition region, the scaling equation is invalid. Thus, the turning point of the external field H_C on the m^2 vs h/m curve reflects the boundary between the first-order transition and the second-order one, as shown in Fig. 6 (b). The H_C vs T is plotted in the inset of 6 (b), which decreases almost linearly with increasing temperature when approaching T_C. The point where the H_C and T_C meet is the H_{TCP}. The linear fitting of the $H_C(T)$ yields $H_{TCP} \approx 3200$ Oe at T_C, which is very close to 3400 Oe obtained by specific heat experiments [30].

As mentioned above, the critical exponents of MnSi indicate a long-range magnetic coupling. However, as can be seen in Table I, the critical exponents of $Fe_{0.8}Co_{0.2}Si$ and Cu_2OSeO_3, which also exhibit a helimagnetic and skyrmion phase transition with similar crystal symmetry, are close to the universality class of the 3D-Heisenberg model [24, 25]. That is to say, the micro-magnetic interactions in $Fe_{0.8}Co_{0.2}Si$ and Cu_2OSeO_3 are of the short-range type. The different critical behaviors of MnSi from $Fe_{0.8}Co_{0.2}Si$ or Cu_2OSeO_3 indicate that the micro-magnetic interactions are intrinsically different. The micro-magnetic interaction may correlate with the transport behaviors of the system. The weak itinerant ferromagnetism in MnSi may probably be related to the long-range magnetic coupling since

it has been proved that the transport behavior is connected to the miro-magnetic interaction in these systems [24].

IV. CONCLUSION

In summary, the critical behavior of the single crystal helimagnet MnSi has been investigated around T_C. We obtained the critical exponents $\beta = 0.242 \pm 0.006$, $\gamma = 0.915 \pm 0.003$, and $\delta = 4.734 \pm 0.006$, which are verified with the Widom scaling law and the scaling equation. The critical exponents of MnSi belong to the universality class of tricritical mean-field theory, which unambiguously indicates a tricritical phenomenon. It is suggested that the field-controlled phase transition from the critical fluctuation induced first-order to second-order should be responsible for the appearance of the tricritical phenomenon in MnSi. Based on these critical exponents, the critical exponent for the correlation length is deduced to be $\nu = 0.688 \pm 0.009$ ($\xi = \xi_0|(T - T_C)/T_C|^{-\nu}$). The tricritical point is determined as $H_{TCP} \approx 3200$ Oe at T_C. The exchange distance is obtained to decay as $J(r) \approx r^{-4.3}$, which suggests a long-range magnetic coupling in MnSi.

V. ACKNOWLEDGEMENTS

This work was supported by the State Key Project of Fundamental Research of China through Grant Nos. 2010CB923403 and 2011CBA00111, the National Natural Science Foundation of China (Grant Nos. U1332140, U1232142, 11004196, 11474290, 11104281, and 11204288).

[1] N. Manyala, Y. Sidis, J. F. DiTusa, G. Aeppli, D. P. Young, Z. Fisk, Nature (London) **404,** 581 (2000).

[2] C. Pfleiderer, S. R. Julian, G. G. Lonzarich, Nature (London) **414,** 427 (2001).

[3] H. Watanabe, S. A. Parameswaran, S. Raghu, A. Vishwanath, Phys. Rev. B **90,** 045145 (2014).

[4] C. Pfleiderer, G. J. McMullan, S. R. Julian, G. G. Lonzarich, Phys. Rev. B **55,** 8330 (1997).

[5] U. K. Roβler, A. N. Bogdanov, C. Pfleiderer, Nature (London) **442,** 797 (2006).

[6] S. Muuhlbauer, B. Binz, F. Jonietz, C. Pfleiderer, A. Rosch, A. Neubauer, R. Georgii, P. Boni, Science **323,** 915 (2009).

[7] W. Munzer, A. Neubauer, T. Adams, S. Muhlbauer, C. Franz, F. Jonietz, R. Georgii, P. Boni, B. Pedersen, M. Schmidt, A. Rosch, C. Pfleiderer, Phys. Rev. B **81,** 041203 (2010).

[8] X. Yu, Y. Onose, N. Kanazawa, J. Park, J. Han, Y. Matsui, N. Nagaosa, Y. Tokura, Nature (London) **465,** 901 (2010).

[9] S. Seki, X. Z. Yu, S. Ishiwata, Y. Tokura, Science, **336,** 198 (2012).

[10] H. F. Du, W. Ning, M. L. Tian, Y. H. Zhang, Phys. Rev. B **87,** 014401 (2013).

[11] A. Neubauer, C. Pfleiderer, B. Binz, A. Rosch, R. Ritz, P. G. Niklowitz, P. Boni, Phys. Rev. Lett. **102,** 186602 (2009).

[12] H. F. Du, J. P. DeGrave, F. Xue, D. Liang, W. Ning, J. Y. Yang, M. L. Tian, Y. H. Zhang, S. Jin, Nano Lett. **14,** 2026 (2014).

[13] N. Nagaosa and Y. Tokura, Nat. Nanotechnol. **8,** 899 (2013).

[14] F. Jonietz, S. Muhlbauer, C. Pfleiderer, A. Neubauer, W. Munzer, A. Bauer, T. Adams, R. Georgii, P. Boni, R. A. Duine, K. Everschor, M. Garst, A. Rosch, Science **330,** 1648 (2010).

[15] X. Z. Yu, N. Kanazawa, W. Z. Zhang, T. Nagai, T. Hara, K. Kimoto, Y. Matsui, Y. Onose, Y. Tokura, Nat. Commun. **3,** 988 (2012).

[16] A. Fert, V. Cros, J. Sampaio, Nat. Nanotechnol. **8,** 152 (2013).

[17] J. S. White, K. Prsa, P. Huang, A. A. Omrani, I. Zivkovic, M. Bartkowiak, H. Berger, A. Magrez, J. L. Gavilano, G. Nagy, J. Zang, H. M. Ronnow, Phys. Rev. Lett. **113,** 107203 (2014).

[18] P. Bak and M. H. Jensen, J. Phys. C: Solid St. Phys. **13,** L881 (1980).

[19] A. Bauer and C. Pfleiderer, Phys. Rev. B **85,** 214418 (2012).

[20] H. Wilhelm, M. Baenitz, M. Schmidt, C. Naylor, R. Lortz, U. K. Roβler, A. A. Leonov, A. N. Bogdanov, J. Phys.: Condens. Matter **24,** 294204 (2012).

[21] C. Pappas, E. Lelievre-Berna, P. Falus, P. M. Bentley, E. Moskvin, S. Grigoriev, P. Fouquet, B. Farago, Phys. Rev. Lett. **102,** (2009) 197202.

[22] S. V. Grigoriev, N. M. Potapova, S. A. Siegfried, V. A. Dyadkin, E.V. Moskvin, V. Dmitriev, D. Menzel, C. D. Dewhurst, D. Chernyshov, R. A. Sadykov, L. N. Fomicheva, A.V. Tsvyashchenko, Phys. Rev. Lett. **110,** 207201 (2013).

[23] S. V. Grigoriev, S. V. Maleyev, E. V. Moskvin, V. A. Dyadkin, P. Fouquet, H. Eckerlebe,

Phys. Rev. B **81,** 144413 (2010).

[24] W. J. Jiang, X. Z. Zhou, G. Williams, Phys. Rev. B **82,** 144424 (2010).

[25] I. Zivkovic, J. S. White, H. M. Ronnow, K. Prsa, H. Berger, Phys. Rev. B **89,** 060401(R) (2014).

[26] S. A. Brazovskii, Sov. Phys. JETP **41,** 85 (1975).

[27] M. Janoschek, M. Garst, A. Bauer, P. Krautscheid, R. Georgii, P. Boni, C. Pfleiderer, Phys. Rev. B **87,** 134407 (2013).

[28] S. Buhrandt and L. Fritz, Phys. Rev. B **88,** 195137 (2013).

[29] K. Huang, *Statistical Mechanics*, 2nd ed. (Wiley, New York, 1987).

[30] A. Bauer, M. Garst, C. Pfleiderer, Phys. Rev. Lett. **110,** 177207 (2013).

[31] V. A. Dyadkin, S. V. Grigoriev, D. Menzel, D. Chernyshov, V. Dmitriev, J. Schoenes, S. V. Maleyev, E. V. Moskvin, H. Eckerlebe, Phys. Rev. B **84,** 014435 (2011).

[32] A. K. Pramanik and A. Banerjee, Phys. Rev. B **79,** 214426 (2009).

[33] J. Kindervater, W. Hauβler, M. Janoschek, C. Pfleiderer, P. Boni, M. Garst, Phys. Rev. B **89,** 180408(R) (2014).

[34] H. E. Stanley, *Introduction to Phase Transitions and Critical Phenomena* (Oxford University Press, London, 1971).

[35] M. E. Fisher, Rep. Prog. Phys. **30,** 615 (1967).

[36] A. Arrott and J. Noakes, Phys. Rev. Lett. **19,** 786 (1967).

[37] S. N. Kaul, J. Magn. Magn. Mater. **53,** 5 (1985).

[38] N. Khan, P. Mandal, K. Mydeen, D. Prabhakaran, Phys. Rev. B **85,** 214419 (2012).

[39] A. Arrott, Phys. Rev. **108,** 1394 (1957).

[40] S. K. Banerjee, Phys. Lett. **12,** 16 (1964).

[41] D. Bloch, J. Voiron, V. Jaccarino, J. H. Wernick, Phys. Lett. **51A,** 259 (1975).

[42] J. Y. Fan, L. S. Ling, B. Hong, L. Zhang, L. Pi, Y. H. Zhang, Phys. Rev. B **81,** 144426 (2010).

[43] L. Zhang, B. S. Wang, Y. P. Sun, P. Tong, J. Y. Fan, C. J. Zhang, L. Pi, Y. H. Zhang, Phys. Rev. B **85,** 104419 (2012).

[44] L. Zhang, J. Y. Fan, L. Li, R. W. Li, L. S. Ling, Z. Qu, W. Tong, S. Tan, Y. H. Zhang, Europhys. Lett. **91,** 57001 (2010).

[45] L. P. Kadanoff, Physics **2,** 263 (1966).

[46] A. Perumal, V. Srinivas, V. V. Rao, R. A. Dunlap, Phys. Rev. Lett. **91,** 137202 (2003).

[47] D. Kim, B. Revaz, B. L. Zink, F. Hellman, J. J. Rhyne, J. F. Mitchell, Phys. Rev. Lett. **89,** 227202 (2002).

[48] J. Yang, Y. P. Lee, Y. Li, Phys. Rev. B **76,** 054442 (2007).

[49] M. H. Phan, V. Franco, N. Bingham, H. Srikanth, N. Hur, S. Yu, J. Alloys Compd. **508,** 238 (2010).

[50] A. E. Petrova, V. N. Krasnorussky, J. Sarrao, S. M. Stishov, Phys. Rev. B **73,** 052409 (2006).

[51] A. E. Petrova, V. N. Krasnorussky, J. Sarrao, S. M. Stishov, JETP **102,** 636 (2006).

[52] M. Otero-Leal, F. Rivadulla, S. S. Saxena, K. Ahilan, J. Rivas, Phys. Rev. B **79,** 060401 (2009).

[53] M. Chattopadhyay, P. Arora, S. Roy, J. Phys.: Condens. Matter **21,** 296003 (2009).

[54] N. Khan, A. Midya, K. Mydeen, P. Mandal, A. Loidl, D. Prabhakaran, Phys. Rev. B **82,** 064422 (2010).

[55] M. E. Fisher, S. K. Ma, B. G. Nickel, Phys. Rev. Lett. **29,** 917 (1972).

[56] K. Ghosh, C. J. Lobb, R. L. Greene, S. G. Karabashev, D. A. Shulyatev, A. A. Arsenov, Y. Mukovskii, Phys. Rev. Lett. **81,** 4740 (1998).

[57] S. F. Fischer, S. N. Kaul, H. Kronmuller, Phys. Rev. B **65,** 064443 (2002).

[58] S. V. Grigoriev, S. V. Maleyev, A. I. Okorokov, Yu. O. Chetverikov, R. Georgii, P. Boni, D. Lamago, H. Eckerlebe, K. Pranzas, Phys. Rev. B **72,** 134420 (2005).

TABLE I: Comparison of critical exponents of MnSi with different theoretical models and related materials (MAP = modified Arrott plot; ND = neutron diffraction; Hall = Hall effect; AC = ac susceptibility; SC = single crystal; PC = polycrystal; cal = calculated).

Composition	technique	Ref.	T_C(K)	β	γ	δ
$MnSi^{SC}$	MAP	This work	30.5	0.242±0.006	0.915±0.003	4.734±0.006
Tricritical mean-field	theory	[29]	-	0.25	1.0	5.0
Mean-field	theory	[37]	-	0.5	1.0	3.0
3D-Heisenberg	theory	[37]	-	0.365	1.386	4.8
3D-Ising	theory	[37]	-	0.325	1.24	4.82
$MnSi^{PC}$	MAP	[53]	29.67	0.238±0.001	1.20±0.01	6.1 ± 0.1^{cal}
$MnSi^{SC}$	ND	[58]	28.82	0.22(1)	-	-
$Fe_{0.8}Co_{0.2}Si^{PC}$	Hall	[24]	36.0	0.371±0.001	1.38±0.002	4.78±0.01
$Cu_2OSeO_3^{SC}$	AC	[25]	58.3	0.37(1)	1.44(4)	4.9(1)

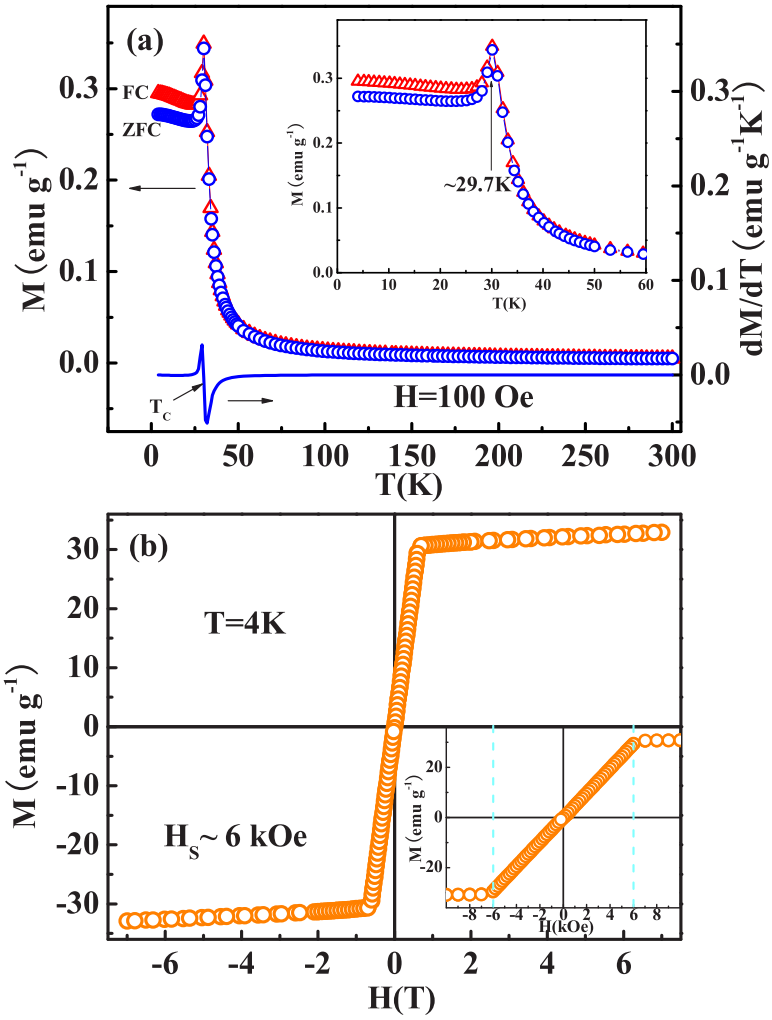

FIG. 1: (Color online) (a) The temperature dependence of magnetization $[M(T)]$ for MnSi (the inset shows the magnification of the transition); (b) the isothermal magnetization $[M(H)]$ at 4 K (the inset gives that in the lower field region).

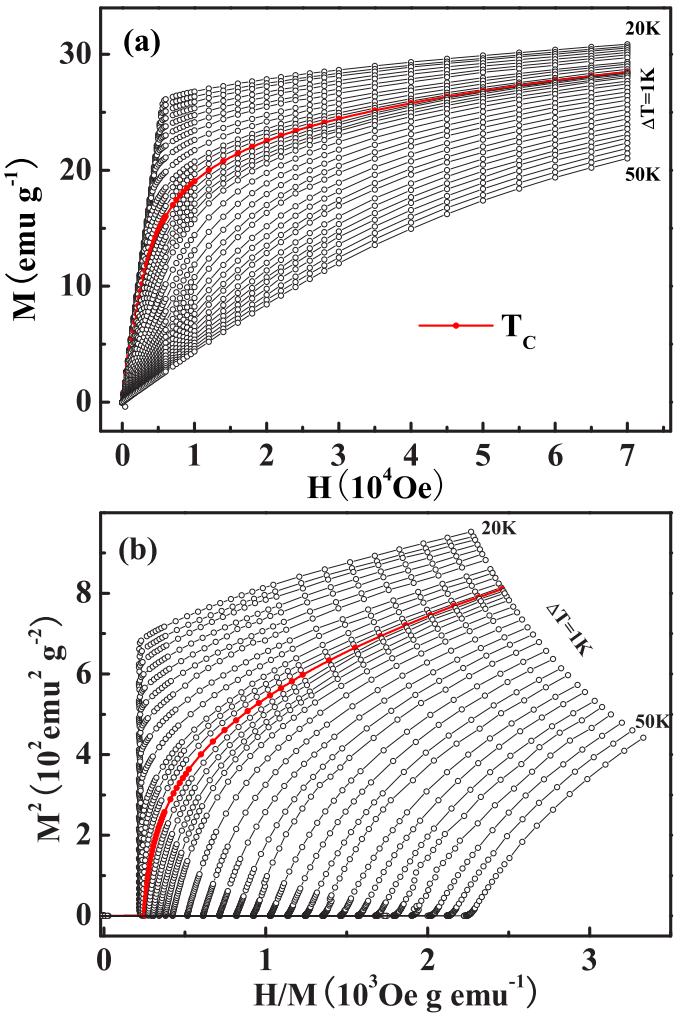

FIG. 2: (Color online) (a) The initial magnetization around T_C for MnSi; (b) the Arrott plots of M^2 vs H/M (the $M(H)$ curves are measured at interval $\Delta T = 1$ K, and $\Delta T = 0.5$ K approaching T_C).

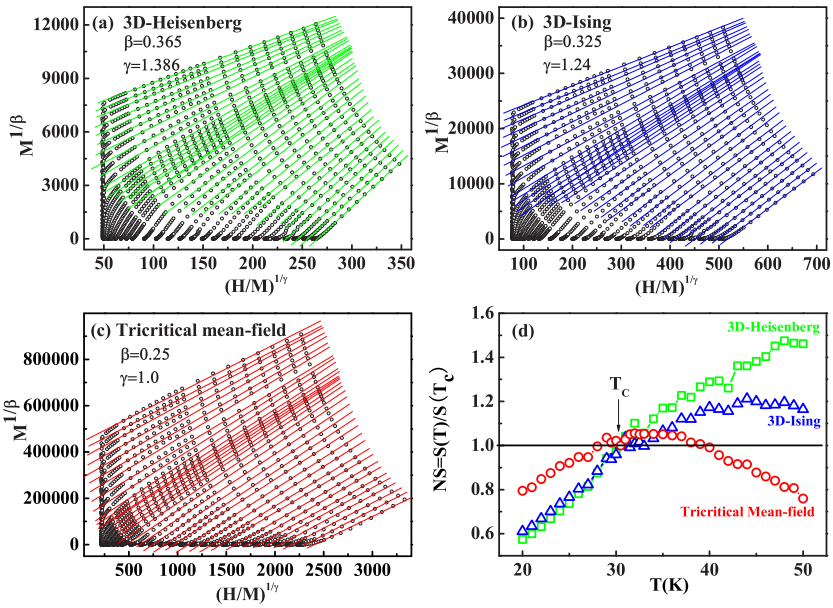

FIG. 3: (Color online) The isotherms of $M^{1/\beta}$ vs $(H/M)^{1/\gamma}$ with (a) 3D-Heisenberg model; (b) 3D-Ising model; (c) tricritical mean-field model; (d) the normalized slopes $[NS = S(T)/S(T_C)]$ as a function of temperature.

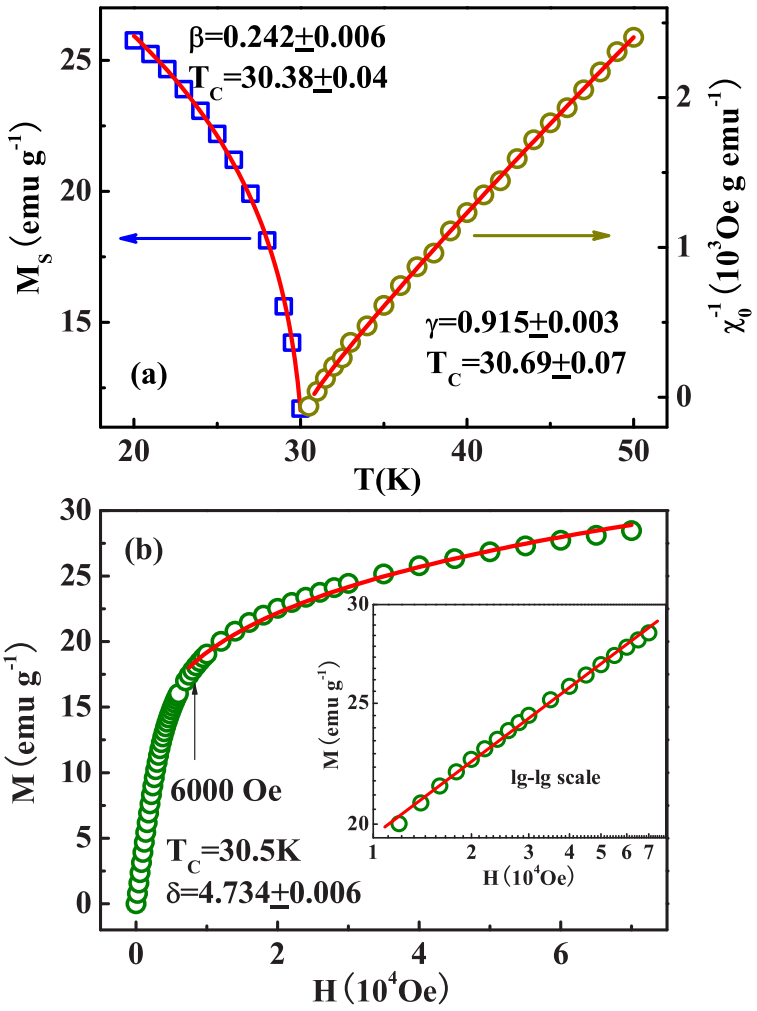

FIG. 4: (Color online) (a) The temperature dependence of M_S and ${\chi_0}^{-1}$ for MnSi; (b) the isothermal $M(H)$ at T_C with the inset plane on the $\lg - \lg$ scale (the solid curves are fitted).

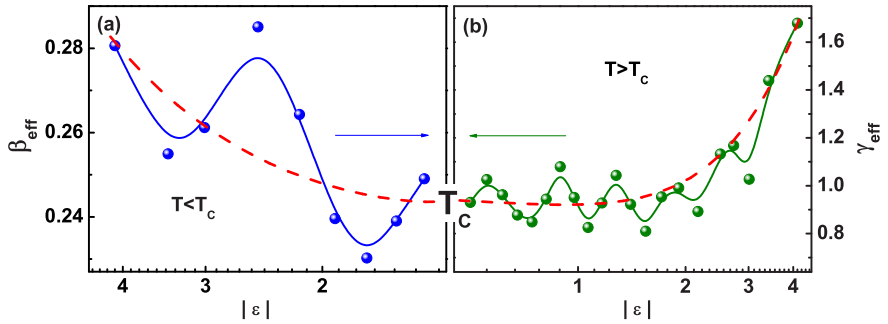

FIG. 5: (Color online) Effective exponents (a) β_{eff} and (b) γ_{eff} as a function of the reduced temperature ε for MnSi (dashed curves are guided on eye).

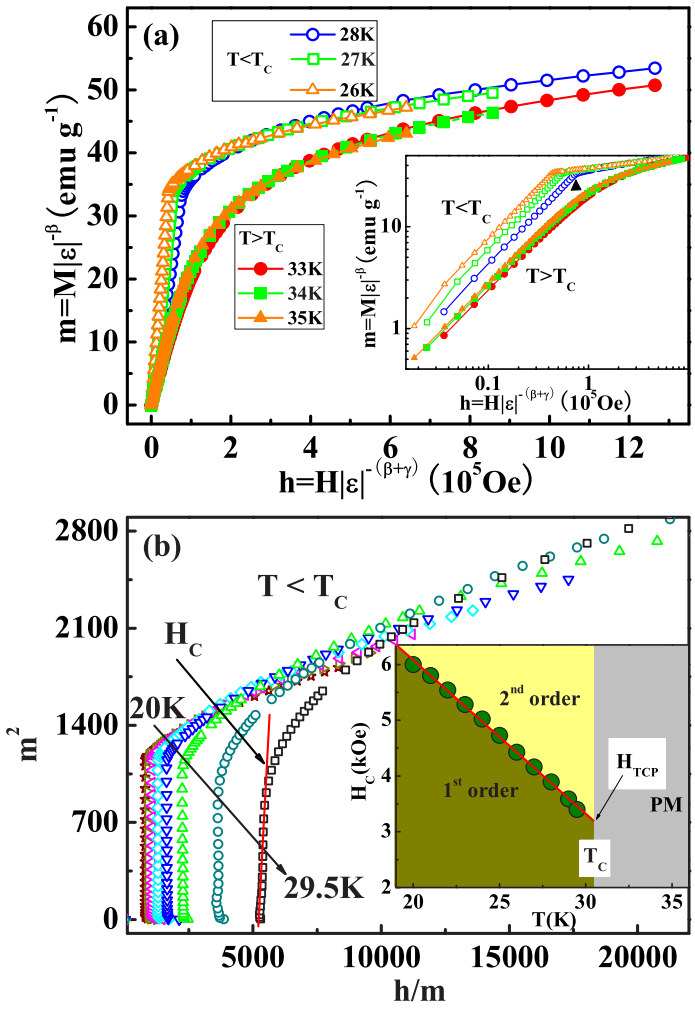

FIG. 6: (Color online) (a) Scaling plots of renormalized magnetization m vs renormalized field h around the critical temperatures for MnSi (only several typical curves are shown); (b) m^2 vs h/m below T_C in lower field region (the inset plot the H_C vs T with the linearly fitting solid line).